5th International Conference on Experimental Fluid Mechanics ICEFM 2018 Munich
Munich, Germany, July 2-4, 2018

Measurements of the wall-shear stress and detection of rare backflow events in turbulent channel flow using the micro-pillar shear stress sensor MPS³

Yiou Liu[1*], Michael Klaas[1], Wolfgang Schröder[1]

[1] Institute of Aerodynamics, RWTH Aachen University, Aachen, Germany

[*] y.liu@aia.rwth-aachen.de

Abstract

The present work investigates the wall-shear stress and the corresponding near-wall rare backflow events in turbulent channel flow measured using the micro-pillar shear-stress sensor (MPS³) at Reynolds numbers of $Re_\tau = 860$ and $1,300$. The results provide experimental evidence of the extreme wall-normal velocities as well as the backflow events.

1 Introduction

The wall-shear stress (WSS) is of vital significance for wall-bounded turbulent flows. On the one hand, the mean WSS τ_w defines the friction velocity u_τ, which serves as a fundamental parameter for the viscous scaling; on the other hand, due to the intermittent nature of turbulent flows, the statistics and dynamics of the WSS fluctuations are direct indicators of the near-wall mechanisms and flow structures, which consequently offers the possibility for the development and extension of theoretical models. As the dependence of the root-mean-squared (rms) fluctuations of the WSS on the Reynolds number evidences the influence from the outer structures (Diaz-Daniel et al. (2017)), such large-scale structures leave their footprints on the WSS distribution.

A study of the WSS distribution allows for the analysis of the near-wall extreme events. These events, characterized by negative streamwise velocities and/or large wall-normal velocity fluctuations, locating around the tails of the probability distribution function (PDF) of the respective velocity components at the wall, are supposed to be associated with the outer large-scale structures. These events have been detected and extensively analyzed based on the data from numerical simulations for different flow cases, e.g., turbulent channel flow by Lenaers et al. (2012) and turbulent boundary layers by Diaz-Daniel et al. (2017). However, experimental verifications of the existence of backflow events were only recently reported for turbulent boundary layers by Brücker (2015), Li et al. (2017a), Li et al. (2017b), and Willert et al. (2018).

This paper presents experimental evidence for the backflow and the extreme wall-normal velocity events in turbulent channel flow based on the WSS data measured using the MPS³ sensor. The sensor consists of an array of flexible cylinders flush-mounted to the surface that protrude into the viscous sublayer and that bend as a result of the fluid forces. Thus, the two-dimensional WSS values are achieved in high spatial and temporal resolution. For further details please refer to Große and Schröder (2009). The organization of the paper is as follows. In section 2, the experimental setup is described. Section 3 comprises the analysis of the experimental data. While the statistics of the WSS components are discussed in section 3.1, the events with large wall-normal velocity fluctuations and the conditional-averaged traces as well as exemplary WSS distributions are analyzed in section 3.2. In section 3.3, backflow events are presented and the corresponding flow features are discussed. The findings are finally summarized in section 4. Throughout this paper, the variables x, y, and z are used to denote the streamwise, the wall-normal, and the spanwise direction, with u, v, and w representing the respective velocity components. The prime $'$ is used to denote the fluctuating components and the superscript $^+$ is used to denote the viscous scaling.

2 Experimental Setup

All measurements of this study were conducted in an Eiffel-type wind tunnel that provides a fully developed turbulent two-dimensional channel flow (Fig. 1). The test section measures $2h \times w = 100 \times 2000$ mm^2 with a length of $L = 2500$ mm. A MPS³ shear-stress sensor array (8×8 pillars, spacing $L = 300$ µm, diameter $\Phi = 22$ µm, height $L_p = 300$ µm) was flush-mounted on the wind-tunnel sidewall. The flow was investigated for bulk Reynolds numbers of $Re_h = 16,000$ and $25,600$ based on the bulk velocity U_b and the channel half height h, corresponding to friction Reynolds numbers of $Re_\tau \approx 860$ and $1,300$, respectively. The field of view was 2.1×2.1 mm^2, which corresponds to a size of $35l^+ \times 35l^+$ for $Re_\tau = 860$ and $52.5l^+ \times 52.5l^+$ for $Re_\tau = 1,300$ in inner scaling. The pillar tips were illuminated by a laser light-sheet parallel to the wall. A Photron Fastcam SA5 high-speed camera equipped with a K2/Infinity long-distance microscope objective was used to record the displacements of the pillar tips, and the achieved resolution was 0.41 px/µm. The measurement frequency ranged from 500 Hz to 25,000 Hz such that both the mean values and the time-resolved fluctuations could be obtained.

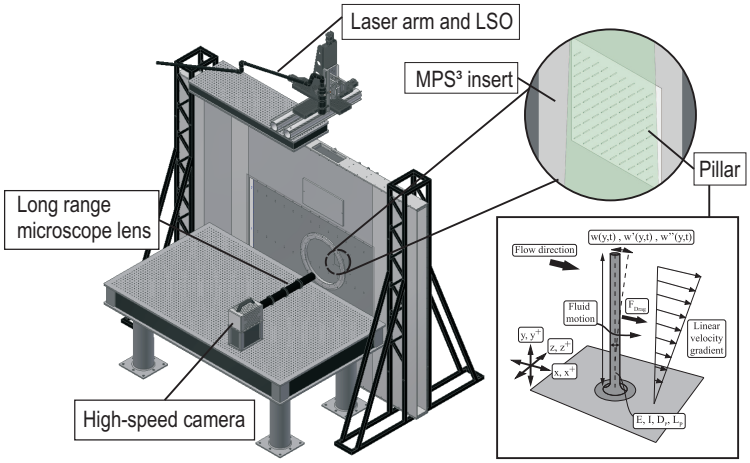

Figure 1: Experimental setup of the turbulent channel flow facility and the measurement principle of the MPS³ sensor.

3 Results

3.1 Wall-shear stress statistics

Table 1 lists the theoretical and measured mean WSS $\tau_{w,theo}$ and $\tau_{w,meas}$, respectively, for both Reynolds numbers and the statistical properties of the WSS derived from the measurements, namely the relative turbulence intensity $\tau^+_{x,rms} = \tau_{x,rms}/\tau_w$, the skewness S_x, and the flatness F_x. In Fig.2(a), the probability distribution functions (PDF) of the normalized streamwise WSS fluctuations $\tau'_x/\tau_{x,rms}$ are juxtaposed with literature data for different Reynolds numbers. The shape of the PDF is highly skewed with a skewness value of $S_x \approx 1$, suggesting that the flow at the wall mainly consists of low-speed fluid. The value of the flatness F_x is suspected to be around 5, and a higher value indicates a larger probability of the occurrence of extreme events. The distributions collapse with each other quite well, except at the tails referring to the events of small probabilities. According to Diaz-Daniel et al. (2017), this feature can be attributed to some dependence on the Reynolds number. Nevertheless, note that the higher order moments vary in the viscous sublayer while the sensor has a length-integrating effect along the wall-normal direction.

Re_τ	U_b [m/s]	$\tau_{w,theo}$ [Pa]	$\tau_{w,meas}$ [Pa]	S_x	F_x	$\tau^+_{x,rms}$	L_p
860	5	0.081	0.089	0.88	4.70	0.28	$5\,y^+$
1300	8	0.180	0.178	1.30	6.42	0.29	$7.5\,y^+$

Table 1: Flow parameters and statistical properties

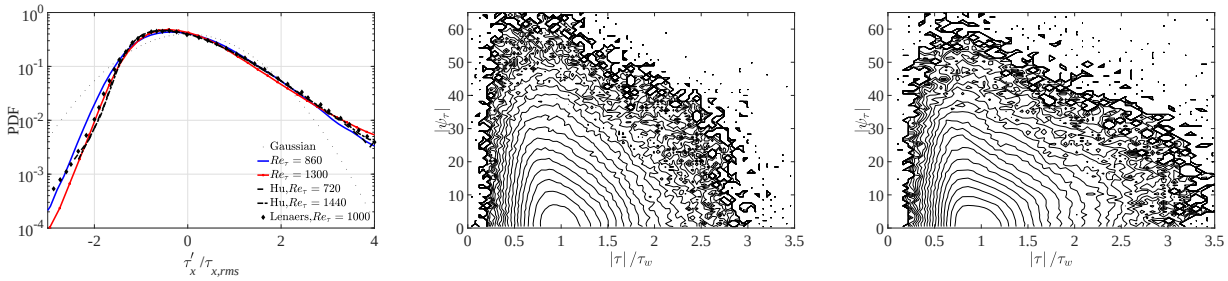

Figure 2: (a) Probability distribution function of the streamwise WSS fluctuations. Present MPS³ results (lines) and literature data from Hu et al. (2006) and Lenaers et al. (2012). (b) (c) Two-dimensional joint-probability density function of the magnitude and angle value of the WSS vector for $Re_\tau = 860$ in (b) and $Re_\tau = 1,300$ in (c) . The 25 contour lines are logarithmically equally spaced between 10^{-6} and 10^{-1}.

Fig.2(b) and (c) show the joint PDFs of the normalized vector magnitude $|\tau|/\tau_w$ and the yaw angle $|\psi_\tau|$ at the two inspected Reynold numbers. The yaw angle of the instantaneous shear stress vector is defined as $|\psi_\tau| = |atan(\tau_z(t)/\tau_x(t))|$. The examination of the yaw angle and the vector magnitude allows for an estimation of the inclination and the intensity of the local WSS field. The maximum of the joint PDF is found to be at the region where the WSS vector possesses a magnitude around the mean value and is of a rather small yaw angle, indicating that the bulk of the flow field motion at the wall is in streamwise direction. Large values of up to $|\tau|/\tau_w > 3$ can be observed at smaller yaw angles, indicating that the occurrence of strong fluctuations is more related to the streamwise motions. However, events with a large yaw angle, i.e., $|\psi_\tau| > 30°$, which correspond to motions tilting against the mean-flow direction, tend to possess smaller magnitudes, suggesting that active spanwise motions represented by large yaw angles are less likely to accompany the strong streamwise motions. The same trend was observed in a numerical study of Diaz-Daniel et al. (2017), who analyzed a zero-pressure gradient (ZPG) turbulent boundary layer using direct numerical simulations (DNS). The contours of the two JPDFs resemble each other, however, some smaller discrepancies can be found, e.g., the slightly broader shape of the JPDF contour for the higher Reynolds number. A broader shape indicates a higher probability of the excursions away from the mean magnitude. In other words, the extreme events of large magnitudes occur more frequently at the higher Reynolds number. This result is in consistency with the larger flatness value at a higher Reynolds number. These aforementioned features concerning the yaw angle and the magnitude at their extreme values, which portray the two-dimensional motions of the WSS, are supposed to be associated with the rare events, i.e., the wall-normal velocity spikes and the local backflow events.

3.2 Extreme wall-normal velocity fluctuation events

Usually, events of extreme fluctuations of the wall-normal velocities near the wall, the so-called positive and negative velocity spikes, are defined using a criterion that sets a threshold for the fluctuations as, e.g., $|v'/v_{rms}| > 5$ by Xu et al. (1996) or $|v'/v_{rms}| > 10$ by Lenaers et al. (2012). In this section, experimental evidence of such events based on the measured WSS vectors is presented and its corresponding relation to the WSS motions is discussed.

Since the MPS³ sensor measures a two-dimensional distribution of the WSS in wall-parallel $x-z$ planes, the wall-normal velocity component can be obtained from continuity considerations (e.g., Große and Schröder (2009)). Assuming a linear velocity profile in the viscous sublayer, the streamwise and spanwise velocity components u and w can be written as:

$$u = \frac{\tau_x}{\mu} y \quad ; \quad w = \frac{\tau_z}{\mu} y \quad , \tag{1}$$

where y denotes the wall-normal distance, i.e., the pillar height, for the current application. Considering the no-slip condition at the wall, the wall-normal velocity is retrieved from the divergence of the in-plane velocity components according to the continuity equation:

$$\frac{\partial v}{\partial y} = -(\frac{\partial u}{\partial x} + \frac{\partial w}{\partial z}) \quad \Rightarrow \quad v = -\frac{1}{\mu}(\frac{\partial \tau_x}{\partial x} + \frac{\partial \tau_z}{\partial z}) \frac{y^2}{2}. \tag{2}$$

This method yields an estimation of the wall-normal velocity component in the wall-parallel measurement plane whose distance from the channel wall is comparable to the pillar height. According to Lenaers et al. (2012), these wall-normal velocity spikes can occur at wall distances of up to $25y^+$. While the pillar heights

($7.5y^+$ for $Re_\tau = 1,300$ and $5y^+$ for $Re_\tau = 860$) are smaller than this distance, the occurrence of such rare events is likely to be detected from the vertical velocity components derived from the measured WSS. Lenaers et al. (2012) applied a criterion of $|v'/v_{rms}| > 10$ for the velocity components at a wall-normal distance of $y^+ \approx 1$ to detect the extreme velocity events. However, the occurrence of extreme velocities decreases rapidly with an increasing wall-normal distance. Thus, a criterion of $|v'/v_{rms}| > 7$ was applied for a wall-normal distance of $7.5y^+$ which corresponds to the pillar height, at a friction Reynolds number of $Re_\tau = 1,300$. The sample rate was $6,000$ Hz. Fig.3 and Fig.4 illustrate the temporal evolution of the conditional averaged positive and negative spikes, respectively. Amongst a total number of $6,989,120$ vertical velocities (8×8 pillars $\times$ $109,205$ snapshots), 430 samples are recognized as the extreme events, yielding a probability of around 0.006%. With respect to the pillar length corresponding to a wall-normal distance of approx. $7.5y^+$, this probability is in good agreement with the findings of Lenaers et al. (2012). The temporal evolution evidences that the positive spikes correlate with the spanwise shear-stress fluctuations, since an abrupt change in the yaw angle occurs simultaneously. The negative spikes, however, seem to be associated with large streamwise fluctuations implying a strong downwash motion, whereas no significant variation in the spanwise motions or the yaw angle is observed. Thus, although both represent the events of a considerably small probability, the negative spikes tend to concentrate at the lower right corner of the Magnitude-Angle JPDF (Fig.2(c)), whereas the positive spikes are likely to be found around the upper left part.

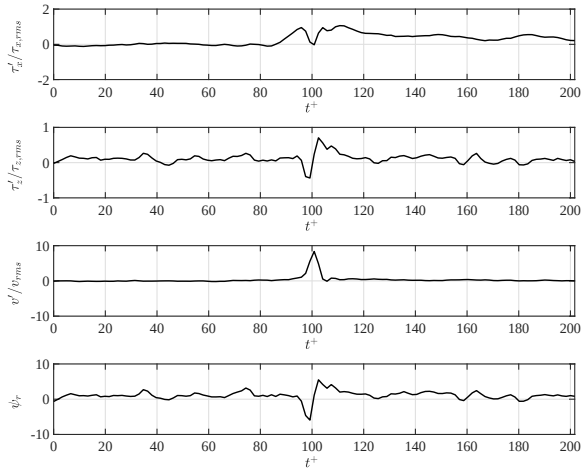

Figure 3: Temporal evolution of the conditional-averaged event of positive wall-normal velocity spikes.

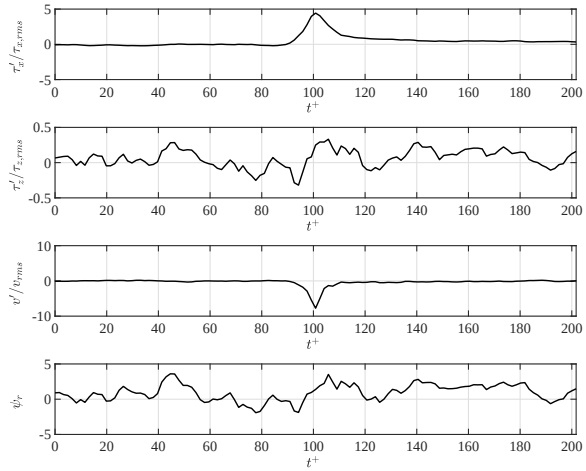

Figure 4: Temporal evolution of the conditional-averaged event of negative wall-normal velocity spikes.

For a better visualization, a typical example of the WSS distribution at $Re_\tau = 1,300$ is shown in Fig. 5. The distributions are constructed from the WSS vectors measured by a spanwise pillar line by applying the Taylor's hypothesis with a given convective velocity of $U_c = 10u_\tau$. The vectors denoting the WSS fluctuations are plotted on the background contour of the fluctuation intensity in the streamwise and wall-normal directions, respectively. In this example, the positive and the negative velocity spikes appear as a pair, with a spatial extent of approx. $50x^+ \times 20z^+$. The negative velocity spike occurs at the position of strong streamwise fluctuations. At the boundary of the negative spike, the flow starts to swirl, turning the positive streamwise fluctuations backwards via strong spanwise motions. These positions represent the intersection region of the high-speed and low-speed fluid, where the positive spike emerges.

3.3 Backflow Events

The backflow events are characterized by a negative value of the streamwise WSS. Unlike the wall-normal velocity spikes, which can penetrate into the flow over a larger distance, the backflow events are found to exist only at the very near-wall region (Lenaers et al. (2012)). The occurrence of such events has been detected for both Reynolds numbers. Note that the total number of the detected backflow events is extremely limited, which could be presumably attributed to the protrusion length and the corresponding length-averaging effect of the sensor. The following WSS features discussed in this section thus rather serve as experimental evidence than statistical reference.

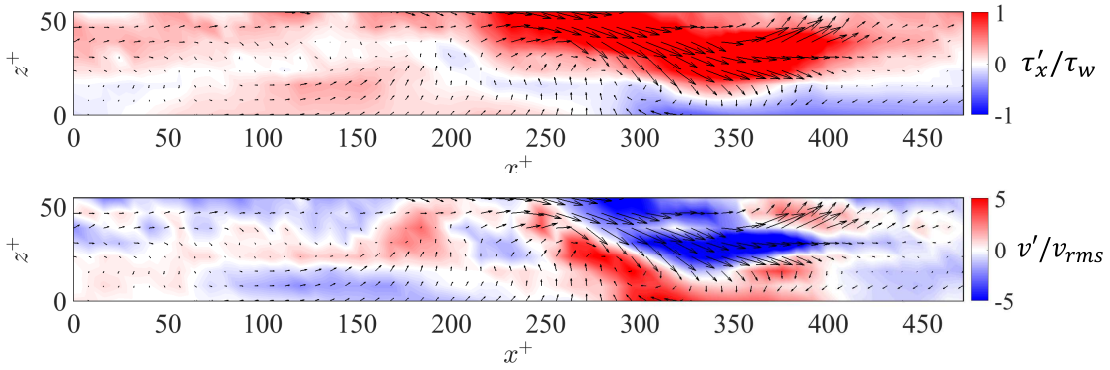

Figure 5: Exemplary WSS distribution for $Re_\tau = 1,300$. Vectors show τ'/τ_w, background contour shows τ'_x/τ_w (top) and v'/v_{rms} (bottom).

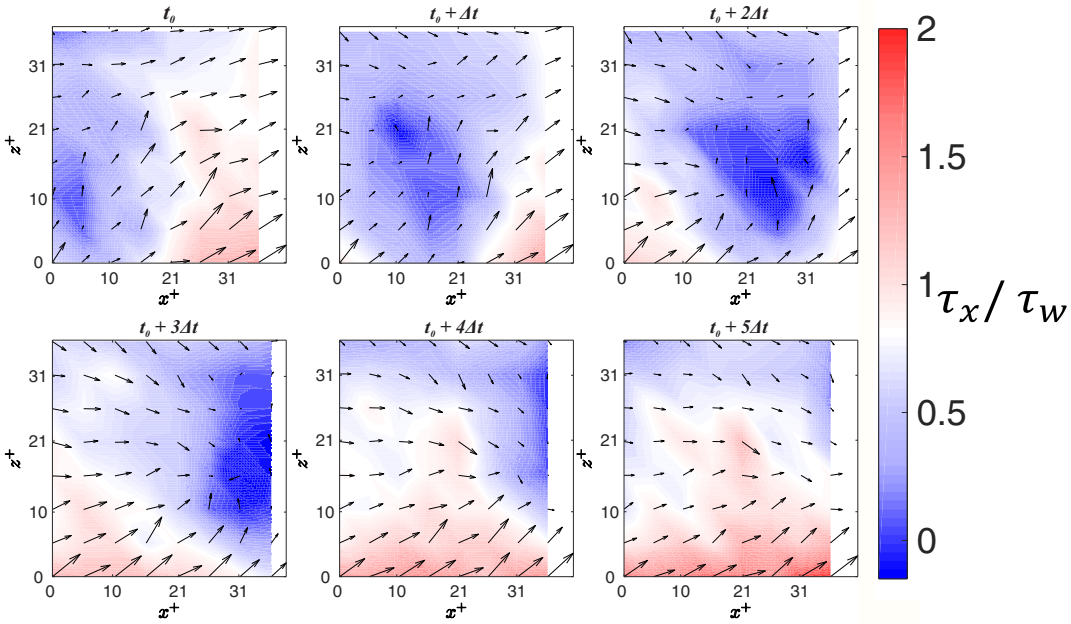

Figure 6: Six timesteps of an exemplary back-flow event visualized using the WSS sensor; $Re_\tau = 860$; $f = 3000$ Hz; $\Delta t = 1.5t^+$; vectors show τ/τ_w, background contour shows τ_x/τ_w, the flow direction is from left to right.

The time-resolved sequence of the WSS field in Fig. 6 shows a reverse-flow region passing through the field of view. In this example, the reverse-flow region first appears as a local negative minimum of the WSS and then develops to a larger area of negative WSS with a size of up to 20 viscous units as it convects downstream. The total duration of this backflow event is around $5.68t^+$. Note that the actual duration of persistence may be underestimated due to the limited field of view ($35l^+ \times 35l^+$) of the MPS³. Along with its convection, the flow vectors tilt towards the direction of the backflow region, i.e. a smaller streamwise magnitude and a larger yaw angle, transforming the streamwise motions into spanwise direction. While this specific instance of backflow region is found to stem from the low-speed fluid, other detected instances demonstrate that the backflow events can also result from the high-speed fluids, of which the mutual characteristics reside in the strong spanwise motion. This finding is in consent with that of Diaz-Daniel et al. (2017) in a turbulent boundary layer, showing that the rare negative events of τ_x can be associated with the extreme values of τ_z.

According to equation (2), the wall-normal velocity is influenced by the local WSS gradient in the sense of continuity. Thus, the bypass of the backflow region, as related to strong spanwise WSS motions, is likely to cause the variation of the local WSS gradient, which consequently alters the local wall-normal velocity. The backflow events are, hence, supposed to have a three-dimensional structure that the size in the $x-z$ plane changes simultaneously with its wall-normal extension as the backflow region convects downstream. Such

variation of the size of backflow region in the $x-z$ plane can be observed in Fig. 6. A three-dimensional feature can be considered as a process of energy exchange between the flow at the wall and the outer part, indicating that the backflow region is not only influenced by the WSS fluctuations at the wall, but also by the velocity fluctuations in the wall-normal direction. Diaz-Daniel et al. (2017) presumed that the negative events of τ_x may be induced by the passing of quasi-streamwise vortices attached to the wall, which are tilted to the x direction. Such three-dimensional features can also be observed from the snapshots of the temporal flow field in the $x-y$ plane visualized by Willert et al. (2018) using PIV. In these measurements, the wall-normal extension of the reverse-flow spot does not remain constant.

4 Conclusion

In this paper, the statistics and distribution of the WSS in turbulent channel flow have been investigated, of which the WSS behavior associated with the near-wall events has been paid special attention.

The probability distribution functions (PDF) of the WSS at two Reynolds numbers show good agreement. The joint-PDF of the magnitude and yaw angle gives an estimate of the WSS vector alignment, and the slightly broader contour at the higher Reynolds number indicating higher intermittency conforms a larger flatness value.

The wall-normal velocity was estimated from the measured WSS. Events corresponding to the positive and negative velocity spikes have been conditional-averaged, respectively. While the positive spikes are likely to co-occur with strong spanwise motions, the negative spikes tend to accompany large streamwise motions. The alignments of the WSS vectors corresponding to the two different spikes locate at different regions of the Magnitude-Angle JPDF. Evidence of backflow events has been found, and these events are observed to be associated with strong spanwise motions. The downstream convection of such backflow regions is supposed to be a three-dimensional motion.

Since both the extreme wall-normal velocity events and the backflow events are near-wall motions, the probability of their existence decreases drastically away from the wall. Note that the sensor has a protrusion length comparable to the viscous sublayer thickness. Thus, the number and strength of the detected events may be underestimated due to the length-integrating effect. The application of shorter pillars may suggest a possible solution.

References

Brücker C (2015) Evidence of rare backflow and skin-friction critical points in near-wall turbulence using micropillar imaging. *Physics of Fluids* 27:031705

Diaz-Daniel C, Laizet S, and Vassilicos JC (2017) Wall shear stress fluctuations: Mixed scaling and their effects on velocity fluctuations in a turbulent boundary layer. *Physics of Fluids* 29:055102

Große S and Schröder W (2009) Wall-Shear stress patterns of coherent structures in turbulent duct flow. *Journal of Fluid Mechanics* 633:147–158

Hu Z, Morfey CL, and Sandham ND (2006) Wall Pressure and Shear Stress Spectra from Direct Simulations of Channel Flow. *AIAA Journal* 44:1541–1549

Lenaers P, Li Q, Brethouwer G, Schlatter P, and Örlü R (2012) Rare backflow and extreme wall-normal velocity fluctuations in near-wall turbulence. *Physics of Fluids* 24:035110

Li W, Roggenkamp D, Jessen W, Klaas M, and Schröder W (2017a) Detection of rare back flow events in zero-pressure gradient turbulent boundary layers using micro-PTV/PIV. *The 12th International Symposium on Partical Image Velocimetry, Busan, Korea*

Li W, Roggenkamp D, Jessen W, Klaas M, and Schröder W (2017b) Reynolds number effects on the fluctuating velocity distribution in wall-bounded shear layers. *Measurement Science and Technology* 28:015302

Willert CE, Cuvier C, Foucaut JM, Klinner J, Stanislas M, Laval JP, Srinath S, Soria J, Amili O, Atkinson C, Kähler CJ, Scharnowski S, Hain R, Schröder A, Geisler R, Agocs J, and Röse A (2018) Experimental evidence of near-wall reverse flow events in a zero pressure gradient turbulent boundary layer. *Experimental Thermal and Fluid Science* 91:320–328

Xu C, Zhang Z, Den Toonder JM, and Nieuwstadt FT (1996) Origin of high kurtosis levels in the viscous sublayer. Direct numerical simulation and experiment. *Physics of Fluids* 8:1938–1944